Reduced-order model based feedback control of the modified Hasegawa-Wakatani model

I. R. Goumiri, C. W. Rowley, Z. Ma, D. A. Gates, J. A. Krommes et al.

Citation: Phys. Plasmas **20**, 042501 (2013); doi: 10.1063/1.4796190
View online: http://dx.doi.org/10.1063/1.4796190
View Table of Contents: http://pop.aip.org/resource/1/PHPAEN/v20/i4
Published by the American Institute of Physics.

Reduced-order model based feedback control of the modified Hasegawa-Wakatani model

I. R. Goumiri,[1,a)] C. W. Rowley,[1] Z. Ma,[1] D. A. Gates,[2] J. A. Krommes,[2] and J. B. Parker[2]
[1]*Department of Mechanical and Aerospace Engineering, Princeton University, Princeton, New Jersey 08544, USA*
[2]*Princeton Plasma Physics Laboratory, Princeton, New Jersey 08544, USA*

(Received 27 January 2013; accepted 4 March 2013; published online 2 April 2013)

In this work, the development of model-based feedback control that stabilizes an unstable equilibrium is obtained for the Modified Hasegawa-Wakatani (MHW) equations, a classic model in plasma turbulence. First, a balanced truncation (a model reduction technique that has proven successful in flow control design problems) is applied to obtain a low dimensional model of the linearized MHW equation. Then, a model-based feedback controller is designed for the reduced order model using linear quadratic regulators. Finally, a linear quadratic Gaussian controller which is more resistant to disturbances is deduced. The controller is applied on the non-reduced, nonlinear MHW equations to stabilize the equilibrium and suppress the transition to drift-wave induced turbulence. © *2013 American Institute of Physics*. [http://dx.doi.org/10.1063/1.4796190]

I. INTRODUCTION

For several decades, toroidal devices have been used to confine plasmas for the purpose of studying nuclear fusion. During this time, a large number of complex dynamic behaviors have been uncovered in toroidal plasmas, including but not limited to magnetohydrodynamic instability, kinetic instability, and microturbulence.

The consequences of these resulting fluctuations include: non-uniformities, increased transport, and possibly even macroscopic break up. Therefore, eliminating these instabilities and fluctuations by using feedback control tools[1–6] has been a topic of considerable interest. Various theoretical and experimental tools have been developed and applied to plasma devices in order to stabilize unstable modes and reduce transport.[7–12]

The Hasegawa-Wakatani[13,14] (HW) system, which couples plasma density and electrostatic potential through an approximation to the physics of parallel electron motion, is a simple model that describes resistive drift wave turbulence. It was first developed to investigate anomalous edge transport due to collisional drift waves.[15]

Due to nonlinearity, drift waves can self-consistently generate zonal flows, which in turn play a key role in the regulation of the drift-wave turbulence and anomalous transport. Traditionally, the mechanism was argued to be the shearing apart of the drift-wave eddies.[16,17] More recently, another turbulence dissipation mechanism has been proposed involving coupling of the unstable drift waves to damped eigenmodes.[18] This coupling can be catalyzed by the zonal flows.[19] The HW model contains both of these mechanisms.

Several models have been used to study the coupling of drift waves turbulence and zonal flow, including a predator/prey model proposed by Diamond *et al.*[20] a 4-dimensional model derived by Chen *et al.*,[21] or a 10-dimensional model derived by Kolesnikov and Krommes.[22] In this paper, the Modified Hasegawa-Wakatani Model (MHW) is used by Numata *et al.*[23] for turbulence analysis.

Parallel electron motion is important for generating, stabilizing, and destabilizing the zonal flow. That is handled naturally in the 3D HW model. However, for computational tractability, it is useful to study a 2D model, as various authors have done.[23,24] Originally, people just replaced the parallel dissipation operator $-D_{\|}\nabla_{\|}^2$ with a constant (thereby essentially assuming the presence of a single, dominant, nonzero parallel wave number $k_{\|}$). However, that approximation is incorrect for zonal flows, for which $k_{\|} = 0$. Therefore, in the MHW model, the parallel term is taken to vanish for the zonal modes.[24]

To study stabilization of drift wave fluctuations, a linear forcing is introduced into the governing equations as a control actuator and its effect is analyzed both theoretically and numerically.

Before describing the control design for the model, a simplified reduced-order model is built by performing a balanced truncation[25] that retains certain modes. The retained modes are the most important ones in the following step, which is the controller design.

This paper goal is to stabilize the unstable modes of this simple MHW model, assuming that their number is computationally small. In reality, more complex dynamics can occur where these unstable modes are numerous, resulting in intractable chaotic dynamics. There is an abundant literature on chaos control in general dynamical systems,[26–29] but those studies are exclusively focused on controlling chaos through small variations in the system parameters on which the nature of the dynamics depends extensively. The feedback is used only to detect the chaotic dynamics; then on the basis of that information sensitive system parameters are varied until the system makes a transition to a regular dynamical state. This methodology could be attractive for theoretical studies or small laboratory experiments, where feedback power is not an issue. However, for fusion plasmas, changes to parameters such as the plasma pressure gradient are very energy intensive and impractical.

[a)]igoumiri@princeton.edu

In contrast, in this paper, linear feedback plays the key role and is applied directly on the system in order to control it. It is found to have a complete stabilizing effect assuming that the controller is applied at the right time (details will be discussed further).

The remainder of this paper is organized as follows. In Sec. II, the MHW model is introduced for coupling drift wave turbulence and zonal flow, its linearization and its controlled developed version (as a state-space realization) are both derived. In Sec. III, the model reduction methodology and its background is discussed, the different tools of control design are presented in Sec. IV, the simulation setup is given in Sec. V, then the results of application of both Secs. III and IV on the MHW model are shown in Sec. VI. Finally, summary and conclusions are presented in Sec. VII.

II. MODIFIED HASEGAWA-WAKATANI MODEL

As stated in Numata *et al.*,[23] the original HW model does not contain zonal flows when restricted to 2D. This leads to consideration of the MHW model.

It describes the nonlinear dynamics of dissipative drift wave turbulence coupled with zonal flow. It consists of two partial differential equations describing the nonlinear evolution of the ion vorticity ζ and density fluctuations n.

A mean density gradient $dn_0(x)/dx$ is assumed in the direction of $-x$. A constant equilibrium magnetic field $\mathbf{B} = B_0\nabla z$ is assumed. The equations are

$$\frac{\partial\zeta}{\partial t} + \{\varphi,\zeta\} = \alpha(\tilde{\varphi}-\tilde{n}) - \mu\Delta^2\zeta, \tag{1a}$$

$$\frac{\partial n}{\partial t} + \{\varphi, n\} = \alpha(\tilde{\varphi}-\tilde{n}) - \kappa\frac{\partial\varphi}{\partial y} - \mu\Delta^2 n, \tag{1b}$$

where zonal and nonzonal components of a variable f are defined as

$$\text{zonal}: \quad \langle f\rangle \equiv \frac{1}{L_y}\int f dy, \tag{2a}$$

$$\text{nonzonal}: \quad \tilde{f} \equiv f - \langle f\rangle, \tag{2b}$$

where L_y is the periodicity length in y. φ is defined as the electrostatic potential with $\zeta = \Delta\varphi, \Delta = \partial^2/\partial x^2 + \partial^2/\partial y^2$ is the 2D Laplacian, $\{a,b\} \equiv (\partial a/\partial x)(\partial b/\partial y) - (\partial a/\partial y)(\partial b/\partial x)$ is the Poisson bracket, μ is the dissipation coefficient, the background density n_0 is assumed to have a fixed exponential profile, so that the background density gradient $\kappa \equiv (\partial/\partial x)\ln n_0$ is assumed constant, and α is the adiabaticity operator. In this 2D setting, α and μ, and κ are considered to be time- and space-invariant constants. Periodic boundary conditions are used. See Sec. V A for more details.

A. Linearized modified Hasegawa-Wakatani model around zero

For simplicity, the unstable equilibrium point of Eq. (1) is chosen as $(\phi_0 = 0, \zeta_0 = 0, n_0 = 0)$. The linearization about this equilibrium is

$$\frac{\partial\zeta}{\partial t} = \alpha(\tilde{\varphi}-\tilde{n}) - \mu\Delta^2\zeta, \tag{3a}$$

$$\frac{\partial n}{\partial t} = \alpha(\tilde{\varphi}-\tilde{n}) - \kappa\frac{\partial\varphi}{\partial y} - \mu\Delta^2 n. \tag{3b}$$

The equations are rewritten in a matrix notation as

$$\frac{d}{dt}\begin{pmatrix}\zeta\\ n\end{pmatrix} = A\begin{pmatrix}\zeta\\ n\end{pmatrix} = \begin{pmatrix}\alpha\Delta^{-1} - \mu\Delta^2 & -\alpha\\ \alpha\Delta^{-1} - \kappa\dfrac{\partial}{\partial y}\Delta^{-1} & -\alpha - \mu\Delta^2\end{pmatrix}\begin{pmatrix}\zeta\\ n\end{pmatrix}. \tag{4}$$

B. Controlled modified Hasegawa-Wakatani model

The controlled version of the MHW equation is built by considering an additional external electrostatic potential as the control input in the model. It can be realized experimentally by introducing an electrode (a probe) inside the tokamak.[30,31] The total electrostatic potential is written as

$$\varphi_{\text{total}} = \varphi_{\text{int}} + \varphi_{\text{ext}}, \tag{5}$$

where φ_{int} is the internal potential, $\varphi_{\text{ext}} = \Phi u$ is the external potential added as the control input, u is a scalar, and Φ is a given column vector that specifies the external field's spatial distribution.

This external potential is then injected into three of the equations that constitute a basis for the derivation of the MHW equations: the ion continuity, electron continuity, and electron parallel momentum equations as follows. The ion continuity equation becomes

$$\partial_t\tilde{n}_i^{\,G} + V_*\partial_y(\varphi_{\text{int}} + \varphi_{\text{ext}}) + (v_{E\text{int}} + v_{E\text{ext}})\cdot\nabla_\perp\tilde{n}_i^{\,G} = 0, \tag{6}$$

where $\tilde{n}_i^G$ denotes the *internal* ion gyrocenter density fluctuations, the electron continuity equation becomes

$$\partial_t\tilde{n}_e = -V_*\partial_y(\varphi_{\text{int}} + \varphi_{\text{ext}}) - (v_{E\text{int}} + v_{E\text{ext}})\cdot\nabla\tilde{n}_e - \nabla_{||}u_{||e}, \tag{7}$$

the electron parallel momentum becomes

$$u_{||e} = D\nabla_{||}(\varphi_{\text{int}} + \varphi_{\text{ext}} - \tilde{n}_e), \tag{8}$$

where V_* is the diamagnetic velocity, v_E is the $E\times B$ velocity, $\tilde{n}_e$ is the electron density fluctuations, and $\nabla_\perp = \partial/\partial x + \partial/\partial y$ and $\nabla_{||} = \partial/\partial z$ are, respectively, the gradients perpendicular and parallel to the magnetic field B. Finally, consider the gyrokinetic Poisson equation, which is usually taken to be the statement of charge quasineutrality

$$\tilde{n}_i = \tilde{n}_e. \tag{9}$$

Here, n_i is the *particle* (not gyrocenter) density fluctuation. One has $\tilde{n}_i = \tilde{n}_i^G + \tilde{n}_i^{\text{pol}}$, where n_i^{pol} is the ion polarization density. In the cold-ion limit, $\tilde{n}_i^{\text{pol}} = \rho_s^2\nabla_\perp^2\varphi$. Here, it is appropriate to just use φ_{int}. This can be argued in several

ways. First, it is not hard to see that if one tries to use $\varphi_{\text{int}} + \varphi_{\text{ext}}$, the system is *not controllable* because it will reduce to a simple change of variables, and therefore no perturbation or forcing will be introduced. Second, an external potential should be cancelled by external charges. Those external charges are not described here. Indeed, the physics of a probe (or array of probes) inserted into a plasma is entirely nontrivial. It is merely assumed that the external potential can be adjusted at will; the plasma physics associated with the response of the plasma to the probe is not considered. Then, this procedure (using just the internal potential in Poisson's equation) is completely analogous to the standard test-particle calculation that is done in elementary plasma kinetic theory. That is, we will use

$$\tilde{n_i}^G = \tilde{n_e} - \rho_s^2 \nabla_\perp^2 \varphi_{\text{int}}. \tag{10}$$

After manipulation, the controlled linearized Modified Hasegawa-Wakatani equations are deduced

$$\frac{\partial}{\partial t}\zeta = \alpha(\tilde{\varphi} - \tilde{n}) + \alpha\tilde{\varphi}_{ext} - \mu\Delta^2\zeta, \tag{11a}$$

$$\frac{\partial}{\partial t}n = \alpha(\tilde{\varphi} - \tilde{n}) + \alpha\tilde{\varphi}_{ext} - \kappa\frac{\partial\varphi}{\partial y} - \kappa\frac{\partial\varphi_{ext}}{\partial y} - \mu\Delta^2 n. \tag{11b}$$

It can then be rewritten as seen in Sec. II A, Eq. (4), as

$$\frac{\partial}{\partial t}\begin{pmatrix}\zeta\\ n\end{pmatrix} = A\begin{pmatrix}\zeta\\ n\end{pmatrix} + Bu, \tag{12}$$

where

$$B = \begin{pmatrix}\alpha\tilde{\Phi}\\ \alpha\tilde{\Phi} - \kappa\partial_y\Phi\end{pmatrix}. \tag{13}$$

III. MODEL REDUCTION OF LINEAR TIME-INVARIANT SYSTEMS

In the area of model-based feedback control of fluid flow, substantial developments have taken place in the last decade, for instance, Cattafesta *et al.*[32,33] and Sipp *et al.*[34] In many applications, the focus is on how to apply actuation in order to maintain the flow around a steady state or an orbit of interest, for instance to delay the transition to turbulence.

Model-based linear control theory provides efficient tools for the analysis and design of feedback controllers, such as Linear-Quadratic Regulators (LQR) and Linear-Quadratic-Gaussian (LQG). However, a significant challenge is that models for flow control problems are often very high dimensional $O(10^{5\sim9})$, so large that it becomes computationally infeasible to apply linear control techniques. To address this issue, model reduction, in which a low-order approximation model is obtained, is widely employed.

In this section, various techniques for constructing reduced-order models are briefly reviewed before concentrating on one method in particular, the balanced truncation, which will be used for the control design.

A. Overview of model reduction techniques

Among many model reduction techniques, such as singular perturbation or Hankel norm reduction methods, the projection-based method, which involves projection of a model onto a set of modes, is a widely used approach. These may be global eigenmodes of a linearized operator,[35] modes determined by proper orthogonal decomposition (POD) of a set of data,[36] and variants of POD, such as including shift modes.[37] In particular, an efficient projection-based method for linear control systems is balanced truncation.[25] Compared to most other methods, including POD, balanced truncation has key advantages, such as a priori error bounds and guaranteed stability of the reduced-order model if the original high-order system is stable.

While this method is computationally intractable for systems with very large state spaces ($\gtrsim 10^5$), recently an algorithm for computing approximate balanced truncation from snapshots of linearized and adjoint simulations has been developed[38] and successfully applied to a variety of high-dimensional flow control problems[39–41] (with state dimension up to 10^7).

In this method, sometimes called balanced POD (BPOD), one obtains two sets of modes (primary and adjoint) that are bi-orthogonal, and uses those for projection of the governing equations. BPOD typically produces models that are far more accurate and efficient than standard POD models, in the sense that the number of modes needed to capture the dynamics in BPOD is much less than that in POD. Detailed comparisons have been given by Rowley[38] and Ilak and Rowley.[39]

One of the difficulties that BPOD users can face occurs when they deal with experimental data: the main restriction is that balanced POD requires snapshots of impulse-response data from an adjoint system, which is not available for experiments. To address this issue, another technique exists, called the eigensystem realization algorithm (ERA).[42] For linear systems, ERA theoretically produces exactly the same reduced-order models as balanced POD, with no need of an adjoint system, and at an order of magnitude lower computational cost.

For simplicity, the numerical problem considered in this paper will have a small dimension state space, so the exact balanced truncation can reasonably be applied without worrying about the computational tractability.

B. Balanced truncation of stable systems

A stable linear time-invariant state-space system is described as follows:

$$\begin{aligned}\dot{x} &= Ax + Bu,\\ y &= Cx,\end{aligned} \tag{14}$$

where $x \in \mathbb{R}^n$ is the high-dimensional state (for instance, the state variables at all grid points of the simulation), $u \in \mathbb{R}^p$ is a vector of inputs (for instance, actuators or disturbances), and $y \in \mathbb{R}^q$ is a vector of outputs (for instance, sensor measurements, or other measurable quantities as linear functions of the state).

For such a system, the concepts of controllability and observability can be defined, which are quantified by a pair of symmetric, positive-semidefinite matrices

$$W_c = \int_0^\infty e^{At} B B^\dagger e^{A^\dagger t} dt, \tag{15a}$$

$$W_o = \int_0^\infty e^{A^\dagger t} C^\dagger C e^{At} dt, \tag{15b}$$

called controllability and observability Gramians, where daggers denote adjoint operators.

The controllability Gramian W_c provides a measure of the influence of input history on the current state (i.e., to what degree each state is excited by inputs), and the observability Gramian W_o measures the influence of an initial state on future outputs with zero control input (i.e., to what degree each state excites future outputs). The larger eigenvalues of the controllability (observability) Gramian correspond to the more controllable (observable) states.

A balanced truncation involves first a coordinate transformation T, called the balancing transformation, which simultaneously diagonalizes these matrices. That is, under a change of coordinates $x = Tz$, the transformed Gramians become

$$T^{-1} W_c (T^{-1})^\dagger = T^\dagger W_o T = \Sigma, \tag{16}$$

where $\Sigma = \mathrm{diag}(\sigma_1, \ldots, \sigma_n)$. The diagonal entries are called Hankel singular values and are customarily ordered so that $\sigma_1 \geq \cdots \geq \sigma_n \geq 0$.

A reduced-order model may then be obtained by truncating the states that are least controllable and observable. That is, if $T = \begin{bmatrix} T_1 & T_2 \end{bmatrix}$ and $x = Tz = T_1 z_1 + T_2 z_2$, then a reduced-order model is obtained by setting $z_2 = 0$, yielding a model of the form

$$\begin{aligned} \dot{z}_1 &= A_r z_1 + B_r u, \\ y &= C_r z_1. \end{aligned} \tag{17}$$

The resulting reduced-order balanced model retains the most controllable and observable states and is therefore suitable for capturing the input-output dynamics of the original system.

Quantitatively, the balanced truncation procedure guarantees an a priori upper bound of error between the original system and the reduced-order model. If $G(s) = C(sI - A)^{-1} B$ denotes the transfer function of the system (14), and $G_r(s)$ denotes the corresponding transfer function of the approximation Eq. (17), then

$$\|G - G_r\|_\infty < 2 \sum_{k=r+1}^{n} \sigma_r. \tag{18}$$

In addition, any reduced-order model G_r with r states satisfies

$$\|G - G_r\|_\infty > \sigma_{r+1}, \tag{19}$$

where σ_{r+1} is the first neglected Hankel singular value of G. This is a fundamental limitation for any reduced-order model. The two inequalities (18) and (19) provide a priori error bounds which will be used in Sec. VI.

C. Balanced truncation of unstable systems

Balanced truncation has been extended to linear, unstable systems[40,43] by decomposing the system into a stable subsystem and an unstable subsystem.

Consider the state-space system defined in Eq. (14). If it is unstable, the system can be decoupled into an n_s-dimensional stable subsystem and an n_u-dimensional unstable subsystem. Then, the balanced truncation may be applied on the stable subsystem. The number of unstable eigenvalues is typically small (if it is not, then the control task is especially difficult), so this approach is usually computationally feasible.

Consider $R = \begin{bmatrix} R_u & R_s \end{bmatrix}$ being the matrix of right eigenvectors (where the columns of R are eigenvectors) and $L = \begin{bmatrix} L_u \\ L_s \end{bmatrix}$ being the left eigenvectors (where rows of L are eigenvectors). The state x can be expanded as

$$x = x_u + x_s, \tag{20}$$

where $x_u \in \mathbb{R}^n$ is in the unstable eigenspace (image of R_u, a subspace of dimension n_u) and $x_s \in \mathbb{R}^n$ is in the stable eigenspace (image of R_s). The projection onto the stable subspace is then

$$P_s = I - R_u L_u, \tag{21}$$

where R_u and $L_u \in \mathbb{R}^{n \times n_u}$ are matrices of right and left unstable eigenvectors that have been normalized such that $L_u R_u = I_{n_u}$ (and of course, $L_u R_s = 0$). Thus, $x_s = P_s x$.

The reduced-order model is calculated on the stable subspace, so a balancing transformation $T = \begin{bmatrix} T_1 & T_2 \end{bmatrix}$ is found, x_s can then be written

$$x_s = T_1 z_1 + T_2 z_2, \tag{22}$$

where T_1 has r columns, corresponding to the modes kept (so $z_1 \in \mathbb{R}^r$), and T_2 has n–r columns, corresponding to neglected modes (so $z_2 \in \mathbb{R}^{n-r}$). Define also

$$T^{-1} = S = \begin{bmatrix} S_1 \\ S_2 \end{bmatrix}, \tag{23}$$

so that $P_1 = T_1 S_1$ is the projection onto the image of T_1, an r-dimensional subspace of $\mathbb{R}^n$.

The state in the reduced-order model is then

$$x_r = \begin{bmatrix} L_u x \\ z_1 \end{bmatrix} = \begin{bmatrix} L_u \\ S_1 P_s \end{bmatrix} x. \tag{24}$$

In this notation, the approximation to the full state is then

$$\begin{bmatrix} R_u & T_1 \end{bmatrix} x_r = R_u L_u x + T_1 S_1 P_s x = x_u + P_1 x_s. \tag{25}$$

That is, the unstable part of the state is captured exactly, and the stable part is the projection onto the r balancing modes.

Note that, in order to compute x_r, only the right and left *unstable* eigenvectors R_u and L_u need to be computed, not

the stable eigenvectors. This is thus computationally tractable even when the state dimension n is very large, as long as the number of unstable eigenvalues is small.

IV. FEEDBACK CONTROL DESIGN USING REDUCED ORDER MODELS

Once the reduced-order model is obtained and validated, standard techniques from linear control theory can be applied in order to design controllers for the low-dimensional system. These controllers are designed on the reduced models, then applied to the full-dimensional linearized model, and finally tested on to the original nonlinear model to determine if the controller can suppress disturbances in the neighborhood of the unstable equilibrium.

A. Full-state feedback control design

A standard linear control technique is used in order to obtain stabilizing controllers: a linear state feedback $u = -K_r x_r$ is used such that the eigenvalues of $A_r - B_r K_r$ are in the left half of the complex plane. The gain K_r is chosen to minimize the quadratic cost function

$$J[x_r, u] = \int_0^\infty (x_r^\dagger Q x_r + u^\dagger R u) dt, \tag{26}$$

where Q and R are positive weights computed as follows. Q is chosen such that the first term in the integrand above represents a weighted norm of the output $y = C_r x_r$, thus $Q = q * C_r^\dagger C_r$, where q is a adequately chosen weight (scalar). Since u is a scalar (there is only one actuator), the weight R is a scalar too, and so may be taken to be 1 without loss of generality.

Once this controller K_r is designed, it is implemented on both the full linear and nonlinear system. The control implementation steps are sketched in Fig. 1: first compute the reduced-order state x_r, using the expression $x_r = \Psi x$ where

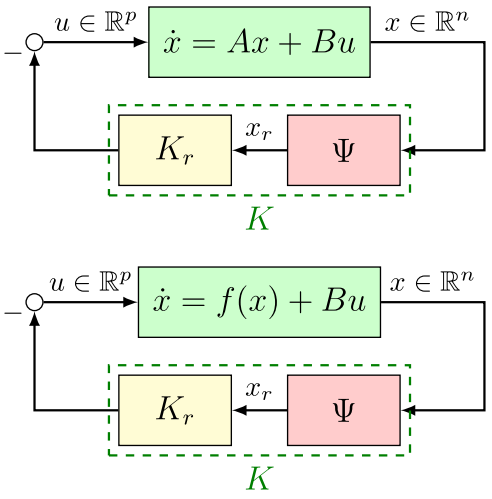

FIG. 1. Schematic of the implementation of the full-state feedback control in the full linear (top) and full non linear (bottom) simulations. The entire state is first projected onto the unstable eigenvectors and the stable subspace of the balanced modes in order to compute the reduced-order state x_r. The state is then multiplied by the gain K, computed based on the reduced-order model using *LQR* to obtain the control input $u = -K_r \Psi x$.

$\Psi = \begin{bmatrix} L_u \\ S_1 P_s \end{bmatrix}$ and T_1 (the transformation matrix), then the control input is given by $u = -K_r x_r$.

B. Observer-based feedback control design

In most engineering applications, the state of the full system is unknown, and thus a full-state feedback controller that updates the control input based on the current state is not directly applicable. Instead, one typically uses an observer-based feedback controller to update the feedback control inputs based on the sensor measurements (outputs).

As before, using the reduced-order model, an observer is designed using a quadratic estimator known as the Kalman filter. This method is optimal if the errors in representing the state x_r and the measurements y are stochastic Gaussian processes. Such errors typically arise from inaccuracies in the model, external disturbances, and sensor noise. The method gives us an estimate $\hat{x}_r$ of the state x_r that is optimal in the sense that it minimizes the mean of the squared error; for more details, see Skogestad and Postlethwaite.[44]

The disturbances w comes from the model truncation and ignoring the nonlinear terms in the reduced-order model (linearization). The sensor noise v (error in measurements) comes from the output projection (the output is the projection of the approximated state onto the finite balanced truncation modes deduced previously).

The reduced-order model dynamics with process and sensor noise included is defined as follows:

$$\begin{aligned} \dot{x}_r &= A_r x_r + B_r u + w, \\ y &= C_r x_r + v. \end{aligned} \tag{27}$$

Again, both disturbances and sensor noise are Gaussian processes whose variances are

$$Q = E(ww^\dagger), \qquad w = P_{\text{bal}} f(x) - P_{\text{bal}} A x, \tag{28a}$$

$$R = E(vv^\dagger), \qquad v = y - C P_{\text{bal}} x, \tag{28b}$$

where $E(.)$ is the expected value, $P_{\text{bal}}(.)$ is the projection onto the Balancing modes, and $P_{\text{bal}} = T_1 S_1$. The resulting estimator has the form

$$\dot{\hat{x}}_r = A_r \hat{x}_r - B_r u - L(y - C_r \hat{x}_r), \quad \hat{y} = C_r x_r, \tag{29}$$

where $\hat{y}$ is the estimated output and L is the observer gain. The estimator is then used along with the full state feedback controller designed previously to determine the control input; a schematic is shown in Fig. 2.

V. SIMULATION SETUP

A. Numerical parameters

The nonlinear and linearized Hasegawa-Wakatani equations are solved in a two-dimensional slab geometry with doubly periodic boundary conditions for simplicity.

The grid size used is 16×16 with the computational domain given by $[0, L_x] \times [0, L_y]$ and $L_x = L_y = 22$, where lengths are normalized by ρ_s, the ion sound Larmor radius

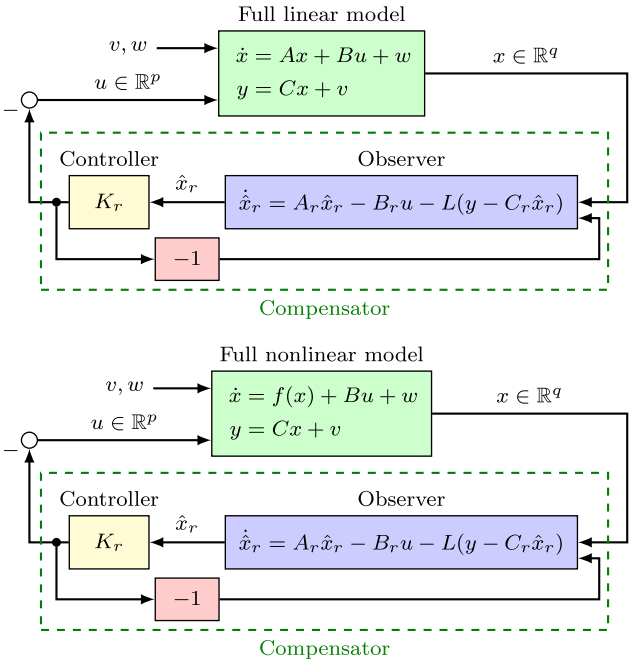

FIG. 2. Schematic of the implementation of the observer-based feedback control in the linear (top) and nonlinear (bottom) simulations. The control input u and the sensor measurements y are used as inputs to the observer, which reconstruct the reduced-order state $\hat{x}_r$. This state is then multiplied by the gain K_r to obtain the control input u. Both the controller and the observer gain K_r and L are computed based on the reduced-order model.

with $\rho_s \equiv v_{si}\omega_{ci}^{-1}$ where $v_{si} \equiv \sqrt{T_e/m}$ is the ion sound velocity in the cold ion limit and T_e is the electron temperature.

The time, ion vorticity, and density fluctuation also have been normalized as follows:

$$\omega_{ci}t \mapsto t, \quad e\varphi/T_e \mapsto \varphi, \quad n/n_0 \mapsto n, \quad x/\rho_s \mapsto x. \tag{30}$$

B. Input and output

The system is actuated by a localized external electrostatic potential in the center of the slab. Its shape is given in Fig. 3. From Eq. (13), the initial condition used for each of the ion vorticity and density fluctuation simulations can be deduced. It is then shown in Fig. 4.

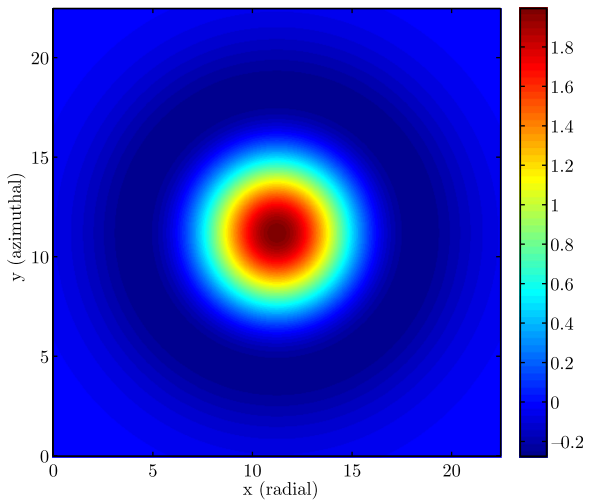

FIG. 3. Actuator localized at the middle of the square plate and modeled as a distribution of the external potential φ_{ext} that is added to the system. It is determined by the function $f(r) = 2(1 - r^2/\gamma^2)\exp(-r^2/\gamma^2)$, where $r^2 = (x - L_x/2)^2 + (y - L_y/2)^2$ and $\gamma = 5$ is a given parameter.

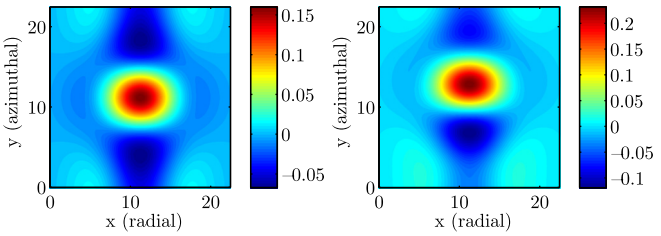

FIG. 4. (Left) The ion vorticity ζ and (right) density fluctuations n of the B-matrix defined in Eq. (14). These two quantities are going to be the initial conditions of the nonlinear, full linear, and reduced model of the MHW equations.

The control objective is to prevent drift wave turbulence by stabilizing the unstable steady states of this model by using the unique actuator defined in Fig. 3, and designing a robust controller. An example of a pair of unstable eigenvectors is shown in Fig. 5.

Table I summarizes the three numerical cases studied in Sec. VI. Both α and μ values are fixed, the density gradient κ is varied for each case, which gives us 3 different cases of right half plane (RHP) (unstable) eigenvalues in the system.

VI. RESULTS

The balanced truncation technique is applied to the MHW equations. In particular, a reduced-order model of the system is obtained, actuated by a localized external electrostatic potential in the center of the slab.

Using this reduced-order model, feedback controllers that stabilize its unstable steady states are developed; first, a full-state feedback controller is designed, then improved by developing a more realistic and practical observer-based controller that uses fewer measurements of the model to reconstruct the entire ion vorticity and density fields.

The goal is to show that these well-known flow control techniques can be applied to this simplified plasma physics model, so that new methods for equilibria stabilization can be obtained, and savings of computational time and memory can

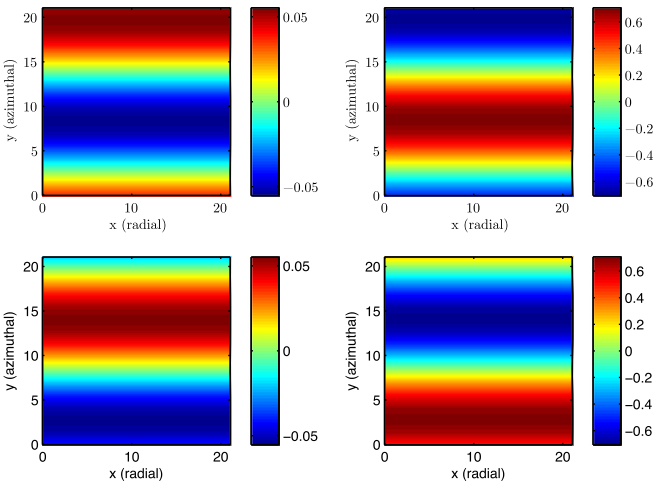

FIG. 5. Representation of the two unstable eigenvectors of the linearized equations. The left part represents its real part, the right its imaginary part.

TABLE I. Summary of the 3 systems that will be reduced then stabilized with only one actuator: for fixed α and μ, only κ is varied and obtain 3 different cases with 2, 4, or 8 right half plane (unstable) eigenvalues.

Case	RHP poles	κ	α	μ
1	2	0.20	0.1	0.2
2	4	0.25	0.1	0.2
3	8	0.28	0.1	0.2

be achieved. Those are very important especially in this domain, where computational requirements are typically large.

A. The nonlinear MHW equations

The study begins by simulating the nonlinear MHW equations, in order to understand the fluctuations that are attempted to be stabilized. The dynamics of coupled drift waves and zonal flows is found.

Figure 6 shows the transition of both ion vorticity and density fluctuation from a horizontally uniform state (drift waves) to an almost vertically uniform state (zonal flow); the sequence then repeats.

Figure 7 shows the same information about the density but focused on one point in the center of the grid, but for longer times, so the coupling between drift waves and zonal flow can be clearly seen in terms of amplitude of one point of density fluctuation, but also in terms of the whole kinetic energy distribution.

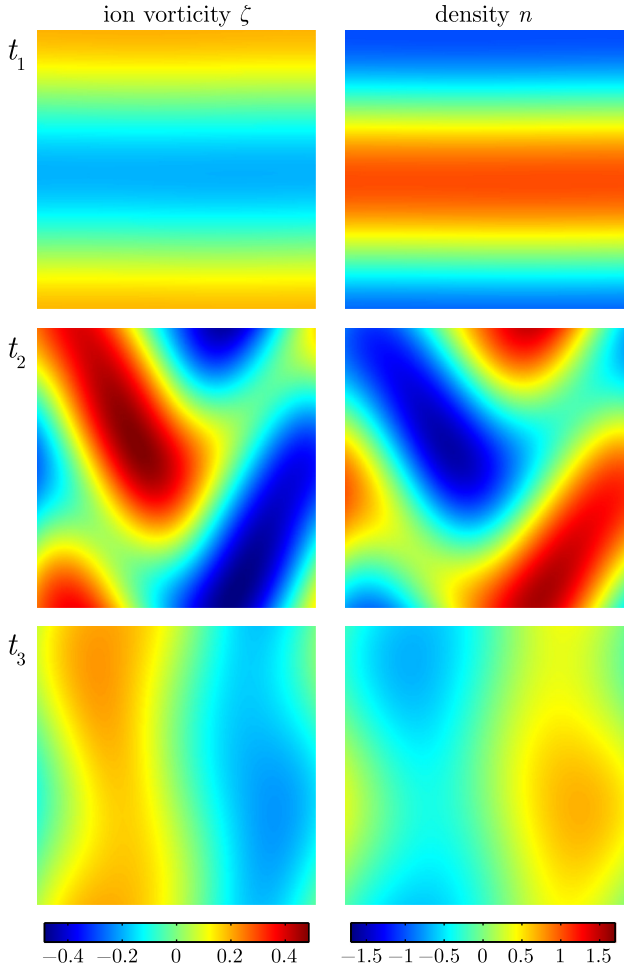

FIG. 6. Ion vorticity and density fluctuation (in color) of the full non linear MHW equations at three successive times with the B-matrix as the initial condition.

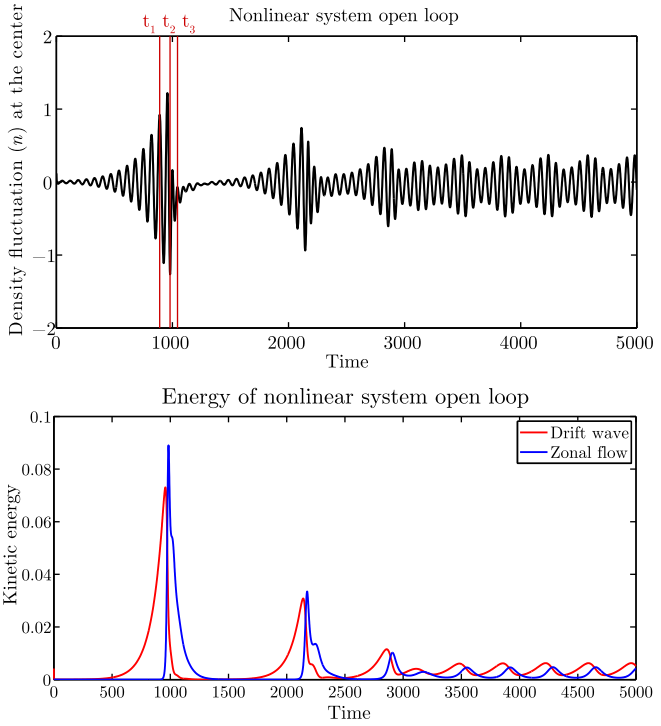

FIG. 7. The output correspond to the density fluctuation that occurs in the center of the square geometry with no control applied on the system.

Having insights into the physics and understanding the coupling of drift waves and zonal flow can help to better design the controller. This idea will be discussed in Sec. VII.

The aim of this paper is not to explain the complex coupling between drift waves and zonal flow; the nonlinear simulation is only used to obtain a big picture of the phenomena in a particular case (here case 1 of Table I), it will help to compare the model before and after applying the controller, and see whether a stabilization of these oscillations is possible near the unstable equilibrium.

B. Reduced-order models and validation

Once the balanced truncation is applied, the error between the original and the reduced-order model is calculated, and compared to its bounds (which were discussed in Sec. III B), and to errors from POD and BPOD models (two other model reduction techniques seen in Sec. III A). The results are represented in Fig. 8. As expected, the balanced truncation method is the one that gives the best approximation (least error) to the original model.

After validation, Table II shows for the three studied cases, the new reduced dimensions obtained, once the balanced truncation is applied. These dimensions have significantly decreased.

C. Full-state feedback control

After designing a reduced-order model as described in Sec. VI B, a full-state feedback controller is then designed,

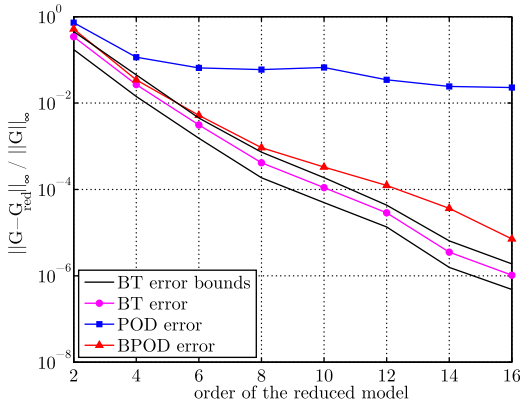

FIG. 8. Error $||G - G_{red}||_\infty / ||G||_\infty$ for balanced truncation (○), balanced POD (△), POD (□), and upper and lower bound for the model reduction scheme.

in which it is assumed that vorticity and density can be measured everywhere.

The controller is built as in Sec. IV, using a LQR with $Q = q * C_r^\dagger C_r$, and implementing it in the full linear system, as well as the full nonlinear system as shown in Fig. 1.

By choosing $q \approx 10$ for the first case study in Table I, the LQR is able to move the right half plane eigenvalues to the left without destabilizing the already stable left half plane ones. q is chosen by numerically experimenting with different values, and then for each value, deduce the LQR controller and visualize the modified eigenvalues of the $A_r - B_r K_r$ matrix. Thus, q is chosen to be the best value that puts the right half plane eigenvalues of both the reduced and full linear models as far to the left as possible without destabilizing the other modes.

Figure 9 compares the density fluctuation in the center of the slab predicted by the reduced, full linear and non linear models with inputs taken from the first case study defined in Tables I and II.

At times $t < 0$, the nonlinear system evolves freely without any control applied on it, the coupling effect is then observed while the reduced and full linear models exhibit just exponentially growing amplitudes that are not shown here. At time $t = 0$, the controller is turned on and immediately for time $t > 0$, the controller damps the oscillations for all three systems, and their controlled dynamics become very close to each other. Therefore, the unstable steady state can be stabilized. More importantly, the reduced-order model predicts the outputs accurately when compared to the full linear or nonlinear system.

Figure 10 compares the density fluctuation in the center of the slab at two different controlling times with inputs taken from the second case study defined in Tables I and II.

TABLE II. Summary of the 3 new reduced systems. r is the dimension of the stable reduced subsystem.

Case	r	Reduced dim. of state
1	4	512↦6
2	6	512↦10
3	12	512↦20

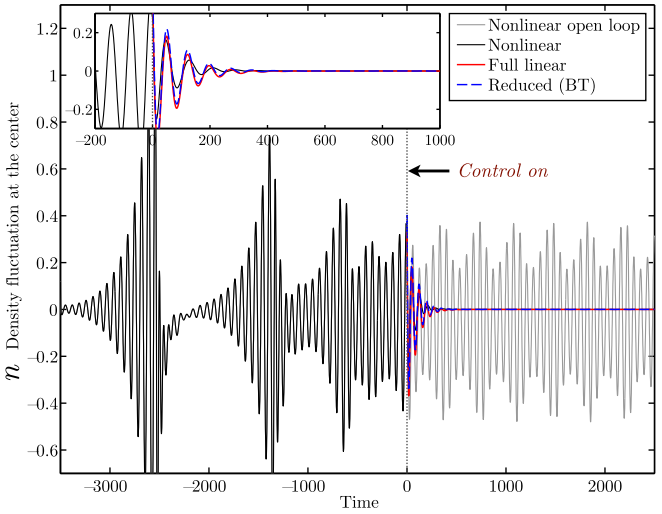

FIG. 9. Full Linear model with 2 eigenvalues in the RHP.

The nonlinear system evolves freely, and then at time $t = 2000$, the controller is turned on (the output response is represented in red), the controller immediately damps the oscillations. But when the controller is turned on at time $t = 2300$ (the output: density in the center, is represented in blue), the controller is not able to damp the oscillations and stabilize the system due to the fact that it went too far from the attraction basin of the equilibrium point.

In order to see that, Fig. 11 (top) shows the distance from the equilibrium for the 2 cases: the one inside the basin of attraction of the equilibrium point (control time at $t = 2000$) and the one outside the basin of attraction of the equilibrium point (control time at $t = 2300$). It can be seen that for the first case, the distance from the zero point tends to converge to zero, whereas in the second case, this distance keeps oscillating and diverges.

Figures 11 (middle and bottom) show the projection of the state on the 7th and 8th modes of the balanced truncation reduced-order model for two different time intervals indicated by the grey areas of the top figure and noted (B) and (C), respectively. These two time intervals are chosen to illustrate when the solution is the closest and furthest of the equilibrium point respectively.

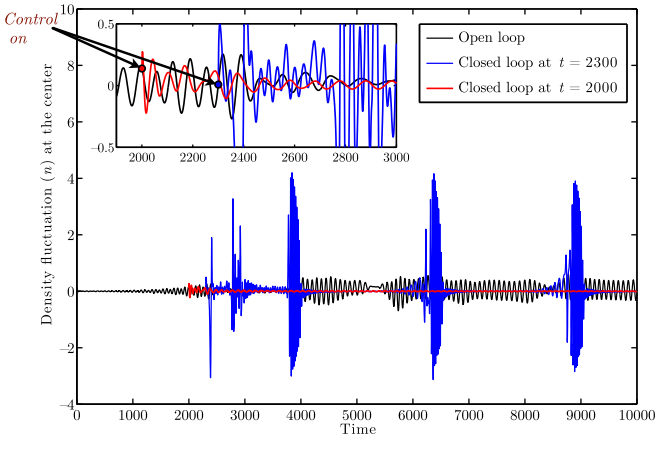

FIG. 10. Full Linear model with 4 eigenvalues in the RHP.

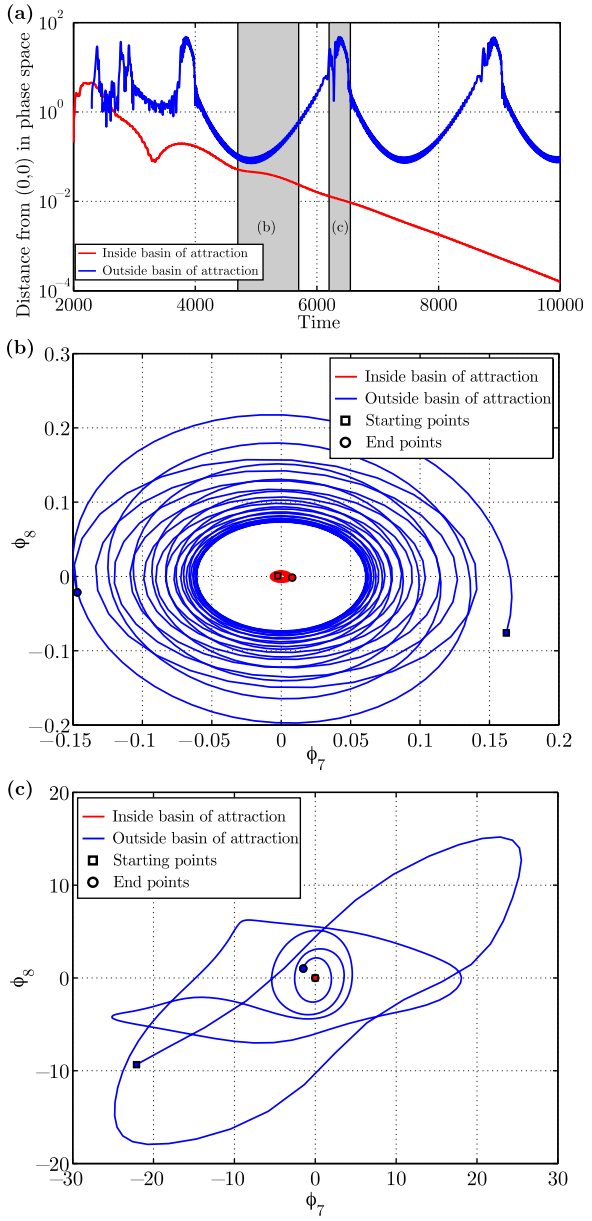

FIG. 11. Full Linear model with 4 eigenvalues in the RHP: phase space plot.

In (B), the stable solution is converging to the equilibrium point at (0,0) whereas the unstable solution is initially approaching and then diverging from (0,0). In (C), the stable solution is still converging to (0,0) whereas the unstable solution is following a complex path, sometimes being apparently close to the equilibrium point, but the projection on different modes would reveal that the distance is much larger.

For the controllable case, Fig. 12 shows a comparison of the reduced-order, full linear and nonlinear centered output of the system. Once again the oscillations are damped and stabilized and the dynamics of all three systems are approximately similar. This demonstrates that the reduced-order model is accurately predicting the full dynamics.

Finally, as the parameter κ increases to 0.28, two more pairs of eigenvalues cross into the right-half plane (simultaneously). One of these pairs turns out to be uncontrollable, as can be verified by the Popov-Belevitch-Hautus (PBH)

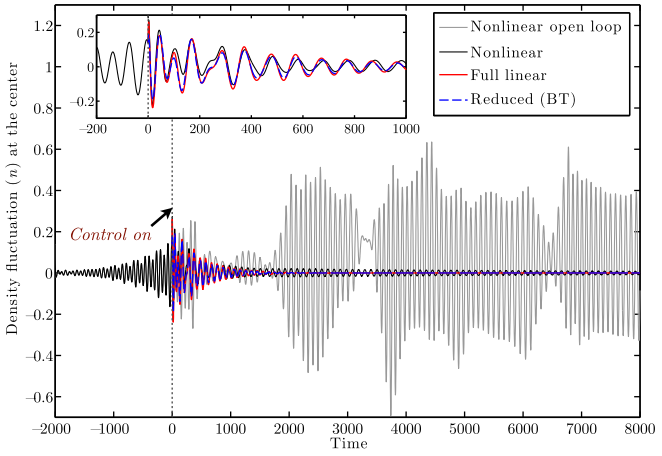

FIG. 12. Full Linear model with 4 eigenvalues in the RHP: inside basin of attraction case.

test,[44] so it is not possible to stabilize the equilibrium with this choice of actuation (shown in Fig. 4).

D. Observer-based feedback control

In practice, the full-state feedback control of the system is not directly useful, since it is not possible to measure the entire ion vorticity and density fluctuation fields. Therefore, considering a more practical approach; the reduced order models obtained from Sec. VI B are used to design dynamic observers based on density fluctuation measurements at a small number of sensor locations.

A 6 (respectively 10) modes reduced order model with 2 (respectively 4) and 4 (respectively 6) modes describing the dynamics on the unstable and stable subspaces, respectively, is used to design the Kalman Filter for producing an optimal estimate of the density fluctuation and ion vorticity fields based on Gaussian approximations of error terms (28a) and (28b). This estimate is then used along with reduced order model controller to determine the control input as shown in Fig. 2. The results of this observer-based controller, which is also called a compensator, are shown for different sensors locations, in Figs. 14 and 15.

Two cases of measurements are considered here

- measurement of the whole density field, thus the C matrix defined in Eq. (14) can be written as

$$C = [0 \quad I], \tag{31}$$

- measurement of only four points of the density field as shown in Fig. 13, thus the C matrix can be written as

$$C = \begin{bmatrix} 0 & \cdots 1 \cdots & & & \\ & & \cdots 1 \cdots & & \\ & & & \cdots 1 \cdots & \\ & & & & \cdots 1 \cdots 0 \end{bmatrix}. \tag{32}$$

Even though these sensors may not be realizable in applications, they serve as a reasonable testing ground for the models.

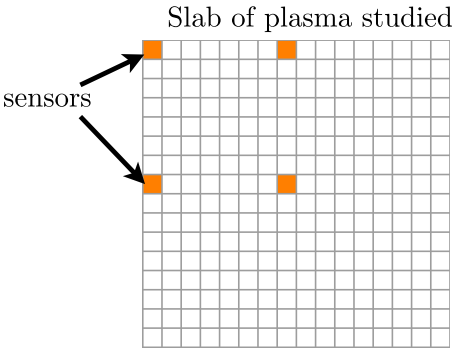

FIG. 13. Sensors location.

Only the second case study results, which contains 4 RHP eigenvalues are shown here, as it contains some interesting constraints on special controlling times when it came about designing the Full state feedback. The measurements will be done one time only of the density field, the other time, 4 points of density only.

Figure 14 shows a comparison of the outputs from the reduced-order, full linear, and nonlinear models when only the density field is measured. The oscillations are still damped and stabilized and the responses agree well, indicating that the reduced-order linear model is a good approximation to the full nonlinear system.

Figure 15 shows us a comparison of the outputs from the reduced-order, full linear, and nonlinear models when only 4 density points are measured. The oscillations are damped and stabilized quicker for the linear models than the nonlinear model where it wiggles a little more and increases before converging to the equilibrium point. The dynamics of the 3 systems are approximately similar until a certain point (a transition behavior of the nonlinear system) but at the end, the controller will be able to control the nonlinear system with only 1 actuator and 4 sensors.

The compensator again stabilizes the unstable equilibrium point and furthermore the observer reconstructs the reduced order model states accurately. Initially, the observer has no information about the states (the initial state estimate

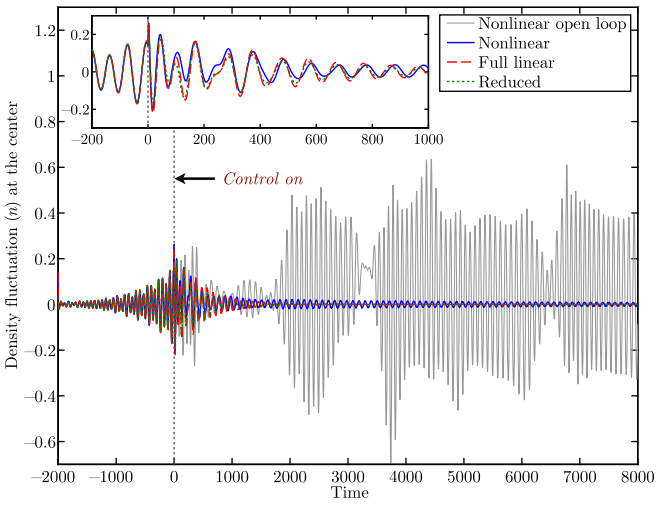

FIG. 14. Output feedback: 4 RHP poles/Full density sensed.

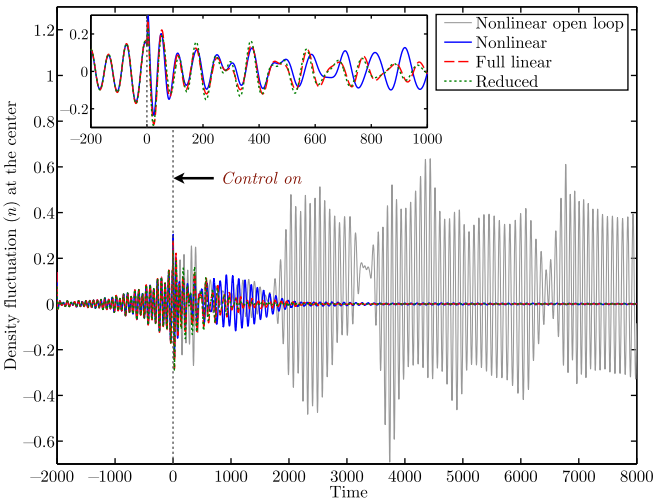

FIG. 15. Output feedback: 4 RHP poles/4 density points sensed only.

is $\hat{x} = 0$), but it quickly converges to and follows the actual states.

Finally to test the robustness of the resulting controller, a Nyquist[44] plot of the loop gain of the input sensitivity function (input loop transfer function) is drawn for each unstable case (2 or 4 right half plane eigenvalues), which corresponds to Figs. (16) and (17), respectively. These plots show the loop transfer function for different outputs considered: measuring density and vorticity (full-state), measuring the full density field, and measuring density at four spatial locations.

The gain (GM) and phase margins (PM) can be deduced from the plots and are given in Table III. It indicates the amount by which the actual dynamics can differ from the model (either in gain or phase), before the closed-loop system loses stability. The cases with only 4 sensors have very small stability margins, indicating that the model needs to be very accurate in order for the controllers to stabilize the equilibrium.

More details about the tools and theory behind it can be found in Astrom and Murray.[45]

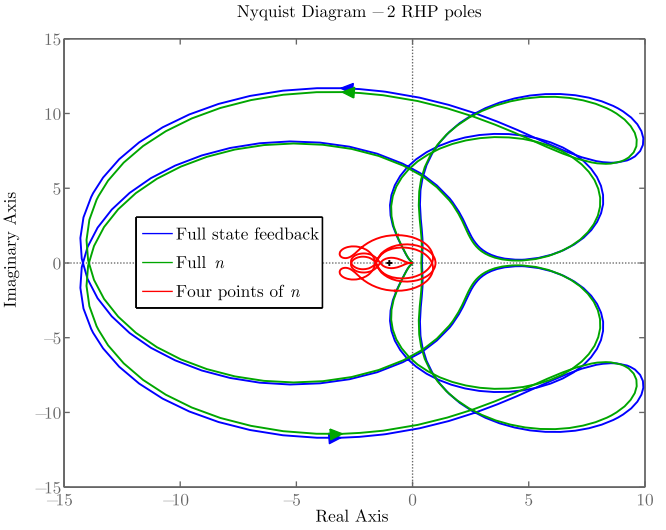

FIG. 16. Nyquist diagram of the loop gain of the input sensitivity function for the unstable case with two right half plane eigenvalues.

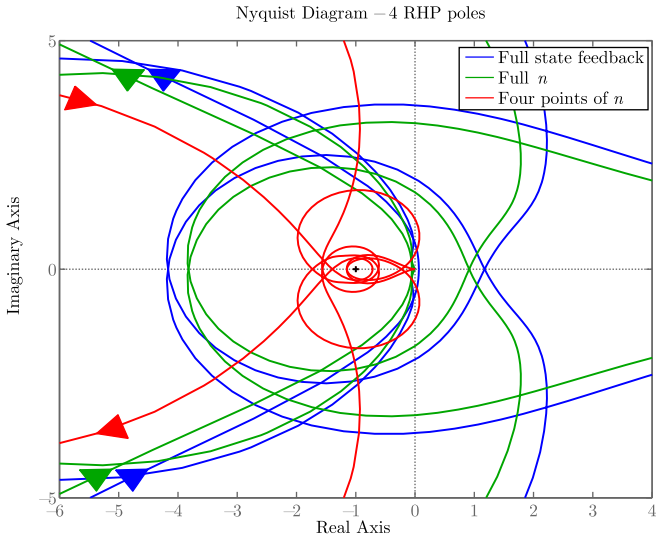

FIG. 17. Nyquist diagram of the loop gain of the input sensitivity function for the unstable case with four right half plane eigenvalues.

TABLE III. GM and PM deduced from the loop gain of the sensitivity function.

Case	Number of sensors	Gain margin	Phase margin
1 pair of	512	82.2	56.6°
RHP e-values	256	41.3	56°
	4	1.26	11.8°
2 pairs of	512	19.3	54.3°
RHP e-values	256	13.5	53°
	4	1.32	13.9°

VII. SUMMARY AND DISCUSSION

The numerical methods for developing a reduced-order model of the input-output dynamics of linear unstable systems are briefly presented in this paper. It is assumed for simplicity that the dimension of the unstable eigenspace is small and the corresponding global modes can be numerically computed. Building the reduced order model treats the unstable subspace exactly, and truncates from the stable subspace only.

These techniques have been frequently used in the fluid control community. The aim of this work has been to introduce and extend these methods to the plasma physics community. Stabilizing controllers based on the reduced-order linear models were developed and applied on unstable state and it was showed that when it works, the models obtained agreed well with the actual simulations. These linear controllers applied to the full nonlinear simulations were fairly successful at suppressing the drift wave turbulence.

A 10 modes reduced-order observer which reconstructed the density and vorticity fields accurately was designed along with an optimal controller and was able to suppress the drift wave turbulence and stabilize the two fields in the neighborhood of the equilibrium point.

Even if the actuator and sensors considered here are not practically realizable, the methodology presented can be extended to a more practical actuation. If given a different equilibrium point than zero, using and amplifying the zonal flow as an actuation would be a smart choice because of its stabilizing effects; once actuated, the zonal flow can reduce the drift wave turbulence as seen in Figs. 6 and 7. This actuation may be a more physical particular way of actuating the plasma slab for this special case where it has an attenuation effect.

Also, adding more actuators and improving their design will provide better control. Here, the whole study was done with only one actuator and in some cases, the stabilization of the whole density and vorticity fields was possible with this unique actuator.

Furthermore, the choice of sensor locations was not optimal either for the given actuator, and different choices for sensor measurements could lead to improved performance.

Finally, a motivation for the choice of this model problem was to show all the possibilities of these control design techniques for a simple model. In the future, for more realistic tokamak models, it may help to make the entire stabilization procedure more automated and rigorous.

ACKNOWLEDGMENTS

The authors would like to acknowledge Professor R. B. White and E. Kolemen for helpful discussions. This work was supported by the U.S. Department of Energy Grant under Contract No. DEAC02-76CH03073.

[1]B. Richards, T. Uckan, A. J. Wootton, B. A. Carreras, R. D. Bengtson, P. Hurwitz, G. X. Li, H. Lin, W. L. Rowan, H. Y. W. Tsui, A. K. Sen, and J. Uglum, Phys. Plasmas **1**, 1606 (1994).
[2]T. Uckan, B. Richards, A. Wootton, R. D. Bengtson, R. Bravenec, B. Carreras, G. Li, P. Hurwitz, P. Phillips, W. Rowan, H. Tsui, J. Uglum, Y. Wen, and D. Winslow, J. Nucl. Mater. **220–222**, 663 (1995).
[3]Z. Kan, Y. Chang-xuang, L. Wan-dong, W. Chao, Z. Ge, and X. Zhi-zhan, Phys. Rev. E **55**, 3431 (1997).
[4]D. D. Blackwell, T. G. Madziwa, D. Arnush, and F. F. Chen, Phys. Rev. Lett. **88**, 145002 (2002).
[5]T. C. Luce, R. J. la Haye, D. Humphreys, C. C. Petty, and R. Prater, AIP Conf. Proc. **595**, 306 (2001).
[6]C. Figarella, A. K. Sen, S. Benkadda, P. Beyer, and X. Garbet, Plasma Phys. Contolled Fusion **45**, 1297 (2003).
[7]A. K. Sen, Phys. Rev. Lett. **76**, 1252 (1996).
[8]J. S. Chiu, M. D. Tinkle, and A. K. Sen, Phys. Rev. E **54**, 2158 (1996).
[9]A. K. Sen, R. Singh, and P. K. Kaw, Phys. Plasmas **4**, 3217 (1997).
[10]J. S. Chiu and A. K. Sen, Phys. Plasmas **4**, 2933 (1997).
[11]A. K. Sen, Phys. Plasmas **5**, 2956 (1998).
[12]A. K. Sen, Phys. Plasmas **1**, 1479 (1994).
[13]A. Hasegawa and M. Wakatani, Phys. Rev. Lett. **50**, 682 (1983).
[14]M. Wakatani and A. Hasegawa, Phys. Fluids **27**, 611 (1984).
[15]W. Horton, Rev. Mod. Phys. **71**, 735 (1999).
[16]W. X. Wang, Z. Lin, W. M. Tang, W. W. Lee, S. Ethier, J. L. V. Lewandowski, G. Wewoldt, T. S. Hahm, and J. Manickam, Phys. Plasmas **13**, 092505 (2006).
[17]K. Itoh, S. Itoh, P. Diamond, T. Hahm, A. Fujisawa, G. R. Tynan, M. Yagi, and N. Nagashima, Phys. Plasmas **13**, 055502 (2006).
[18]P. W. Terry, D. A. Baver, and S. Gupta, Phys. Plasmas **13**, 022307 (2006).
[19]K. D. Makwana, P. W. Terry, and J.-H. Kim, Phys. Plasmas **19**, 062310 (2012).
[20]P. H. Diamond, M. N. Rosenbluth, and F. L. Hinton, "Plasma Physical and controlled Nuclear Fusion Research," in *18th IAEA Fusion Energy Conference, Yokahama, Japan* (1998).
[21]L. Chen, Z. Lin, and R. White, Phys. Plasmas **7**, 3129 (2000).
[22]R. A. Kolesnikov and J. A. Krommes, Phys. Plasmas **12**, 122302 (2005).
[23]R. Numata, R. Ball, and R. L. Dewar, Phys. Plasmas **14**, 102312 (2007).
[24]A. I. Smolyakov, P. H. Diamond, and M. Malkov, Phys. Rev. Lett. **84**, 491 (2000).

[25]B. C. Moore, IEEE Trans. Automatic Control **26**, 17 (1981).
[26]K. Pyragass, Phys. Lett. A **170**, 421 (1992).
[27]E. Ott, C. Grebogi, and J. A. Yorke, Phys. Rev. Lett. **64**, 1196 (1990).
[28]W. L. Ditto, S. N. Rauseo, and M. L. Spano, Phys. Rev. Lett. **65**, 3211 (1990).
[29]T. Shinbrot, W. Ditto, C. Grebogi, E. Ott, M. Spano, and J. A. Yorke, Phys. Rev. Lett. **68** (1992).
[30]T. Klinger, A. Latten, A. Piel, G. Bonhomme, T. Pierre, and T. D. de Wit, Phys. Rev. Lett. **79**, 3913 (1997).
[31]T. Klinger, A. Latten, A. Piel, G. Bonhomme, and T. Pierre, Plasma Phys. Controlled Fusion **39**, B145 (1997).
[32]L. N. Cattafesta, Q. Song, D. R. Williams, C. W. Rowley, and F. S. Alvi, Prog. Aerospace Sci. **44**, 479 (2008).
[33]H. Choi, W. P. Jeon, and J. Kim, Ann. Rev. Fluid Mech. **40**, 113 (2008).
[34]D. Sipp, O. Marquet, P. Meliga, and A. Barbagallo, Appl. Mech. Rev. **63**, 030801 (2010).
[35]E. Akervik, J. Hoepffner, U. Ehrenstein, and D. S. Henningson, J. Fluid Mech. **579**, 305 (2007).
[36]P. Hlomes, J. L. Lumley, and G. Berkooz, *Turbulence, Coherent Structures, Dynamical Systems and Symmetry* (Cambridge University Press, Cambridge, 1996).
[37]B. Noack, K. Afanasiev, M. Morzynski, G. Tadmor, and F. Thiele, J. Fluid Mech. **497**, 335 (2003).
[38]C. W. Rowley, Int. J. Bifurcation Chaos **15**, 997 (2005).
[39]M. Ilak and C. W. Rowley, Phys. Fluids **20**, 034103 (2008).
[40]S. Ahuja and C. W. Rowley, J. Fluid Mech. **645**, 447 (2010).
[41]S. Bagheri, P. Schlatter, P. J. Schmid, and D. S. Henningson, J. Fluid Mech. **624**, 33 (2009).
[42]L. N. Juang and R. S. Pappa, J. Guid. Control Dyn. **8**, 620 (1985).
[43]K. Zhou, G. Salomon, and E. Wu, Int. J. Robust Nonlinear Control **9**, 183 (1999).
[44]S. Skogestad and I. Postlethwaite, *Multivariable Feedback Control: Analysis and Design* (John Wiley and Sons, 2005).
[45]K. J. Astrom and R. M. Murray, *Feedback Systems: An Introduction for Scientists and Engineers* (Princeton University Press, 2008).